Structure of Phosphate Fluorosurfactant Based Reverse Micelles in Supercritical Carbon Dioxide

Sanjib Senapati,† Jason S. Keiper,† Joseph M. DeSimone,† George D. Wignall,‡ Yuri B. Melnichenko,‡ Henrich Frielinghaus,§ and Max L. Berkowitz*,†

Department of Chemistry CB 3290, University of North Carolina, Chapel Hill, North Carolina 27599, Solid State Division, Oak Ridge National Laboratory, Oak Ridge, Tennessee 37831, and Forschungszentrum Jülich GmbH, Institut für Festkörperforschung, D-52425 Jülich, Germany

Received May 15, 2002. In Final Form: June 27, 2002

The existence of microemulsions in the system composed of phosphate-based fluorosurfactant, water, and supercritical CO_2 is demonstrated by small-angle neutron scattering experiments. A computer simulation study performed on a reverse micelle created in this system shows that the micelle remains stable over a 4 ns time period of the simulation. While the data obtained from the experiments provide information about the size of the reverse micelle, the data obtained from the simulations provide additional information about the shape and structure of such a micelle.

Introduction

The formation of water/carbon dioxide microemulsions through the use of fluorosurfactants has been a subject of considerable interest in the recent past. A number of experiments have been carried out to discover suitable surfactants capable of forming water/CO_2 (W/C) microemulsions.[1−12] Phosphate esters are an important family of surfactants that have many industrial applications, and recently, individual phosphate fluorosurfactants have been shown to form W/C microemulsions. Thus Keiper et al.[4] and Steytler et al.[12] reported anionic phosphates capable of W/C microemulsion formation. In both studies, the surfactants allowed for considerable water content in the microemulsions (commonly described in terms of [water]/[surfactant] molar ratio, or W_0) and are thus promising materials for extending W/C microemulsions to a variety of applications. Small-angle neutron scattering (SANS) and small-angle X-ray scattering (SAXS) were used to directly confirm the formation of nanometer-sized microemulsions and to develop a model of colloid shape and structure.

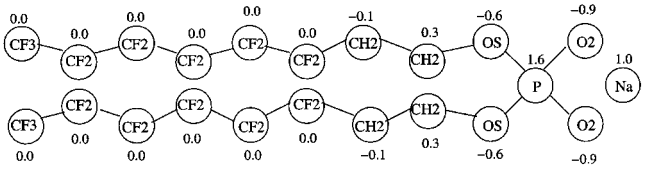

Figure 1. Structure of surfactant **1**. The numbers are the values of the atom-centered point charges.

Although useful information about the structure of reverse micelles present in microemulsions can be obtained from SANS experiments, computer simulations may provide a more detailed molecular description of these aggregates. Recently, Salaniwal et al.[13−15] performed molecular dynamics simulations on a water/dichain surfactant/carbon dioxide system and demonstrated self-assembly of reverse micelles in this system. They also studied the structural properties and the kinetics of aggregation of such micelles. A qualitative agreement between the structural properties of simulated reverse micelles and the experimental results of Eastoe et al.[3] was attained in these simulations.

In this paper, we present the results obtained from a SANS experiment and a molecular dynamics simulation performed on a system containing the double-chain surfactant $(C_6F_{13}(CH_2)_2O)(C_6F_{13}(CH_2)_2O)PO_2^-Na^+$ (surfactant **1**, see Figure 1), water, and supercritical CO_2. As we will see, molecular dynamics simulation data complement the experimental data and provide a wealth of detailed information on the system.

Small-Angle Neutron Scattering Experiments

The presence of microemulsion water pools was directly confirmed using SANS measurements on the KWS2 SANS facility[16] at the FRJ2 reactor in Jülich, Germany, with a 48 × 48 cm² area detector with cell size 0.8 × 0.8 cm² and a wavelength

† University of North Carolina.
‡ Oak Ridge National Laboratory.
§ Forschungszentrum Jülich GmbH.

(1) DeSimone, J. M.; Maury, E. E.; Combes, J. R.; Menceloglu, Y. Z. *Polym. Prepr.* (*Am. Chem. Soc., Div. Polym. Mater. Sci.*) **1993**, *68*, 41.
(2) Harrison, K.; Goveas, J.; Johnston, K. P.; O'Rear, E. A. *Langmuir* **1994**, *10*, 3536−3541.
(3) Eastoe, J.; Bayazit, Z.; Martel, S.; Steytler, D. C.; Heenan, R. K. *Langmuir* **1996**, *12*, 1423−1424.
(4) Keiper, J. S.; Simhan, R.; DeSimone, J. M.; Wignall, G. D.; Melnichenko, Y. B.; Frielinghaus, H. *J. Am. Chem. Soc.* **2002**, *124*, 1834.
(5) DeSimone, J. M.; Maury, E. E.; Menceloglu, Y. Z.; McClain, J. B.; Romack, T. J.; Combes, J. R. *Science* **1994**, *265*, 356−359.
(6) Cooper, A. I.; Londono, J. D.; Wignall, G.; McClain, J. B.; Samulski, E. T.; Lin, J. S.; Dobrynin, A.; Rubinstein, M.; Burke, A. L. C.; Frechet, J. M. J.; DeSimone, J. M. *Nature* **1997**, *389*, 368−371.
(7) Johnston, K. P.; Harrison, K. L.; Clarke, M. J.; Howdle, S. M.; Heitz, M. P.; Bright, F. V.; Carlier, C.; Randolph, T. W. *Science* **1996**, *271*, 624−626.
(8) Lee, C. T., Jr.; Johnston, K. P.; Dai, H. J.; Cochran, H. D.; Melnichenko, Y. B.; Wignall, G. D. *J. Phys. Chem. B* **2001**, *105*, 3540−3548.
(9) Eastoe, J.; Downer, A.; Paul, A.; Steytler, D. C.; Rumsey, E.; Penfold, J.; Heenan, R. K. *Phys. Chem. Chem. Phys.* **2000**, *2*, 5235−5242.
(10) Liu, Z. T.; Erkey, C. *Langmuir* **2001**, *17*, 274−277.
(11) Beckman, E. J. *Science* **1996**, *271*, 613−614.
(12) Steytler, D. C.; Ramsey, E.; Thorpe, M.; Eastoe, J.; Paul A.; Heenan, R. K. *Langmuir* **2001**, *17*, 7948−7950.
(13) Salaniwal, S.; Cui, S. T.; Cummings, P. T.; Cochran, H. D. *Langmuir* **1999**, *15*, 5188−5192.
(14) Salaniwal, S.; Cui, S. T.; Cochran, H. D.; Cummings, P. T. *Langmuir* **2001**, *17*, 1773−1783.
(15) Salaniwal, S.; Cui, S. T.; Cochran, H. D.; Cummings, P. T. *Langmuir* **2001**, *17*, 1784−1792.

10.1021/la025952s CCC: $22.00
Published on Web 08/14/2002

(λ) of 6 Å. A sample−detector distance of 8 m was used to give an overall range of momentum transfer of $0.0054 < Q < 4\pi\lambda^{-1} \sin\theta < 0.042$ Å^{-1}, where 2θ is the angle of scatter. The experiments were conducted by preparing a homogeneous solution of surfactant,[4] D_2O (Cambridge Isotopes), and CO_2 (Air Liquide), thermostated to 35 °C in a stainless steel cell that has been used extensively for previous neutron scattering experiments (23.1 mm path length, 5.6 cm^3 volume).[17,18] Due to the high penetrating power of neutrons, the beam passed through two ~1 cm thick sapphire windows with virtually no attenuation (cell transmission ~ 93%) or parasitic scattering. All data sets were corrected for instrumental backgrounds as described previously[17,18] and normalized to an absolute (±4%) differential cross section per unit sample volume [$I(Q)$ in units of cm^{-1}] by means of precalibrated secondary standards.[19]

For a particle with a core−shell structure suspended in a solvent, after subtracting the CO_2 scattering (~0.04 cm^{-1}), the cross section[20] is given by

$$I(Q) = N_p[(\Delta_1 - \Delta_s)(V_{tot} - V_p) + (\Delta_2 - \Delta_s)(V_p)]^2 P(Q) \quad (1)$$

where Δ_1, Δ_2, and Δ_s are the scattering length densities (SLDs) of the core, shell, and solvent, respectively; N_p is the number of particles per unit volume; V_{tot} and V_p are the total (core plus shell) and core volumes; and $P(Q)$ is the particle form factor [$P(0) = 1$].

The SLDs are 0.025×10^{12}, 0.064×10^{12}, and 0.031×10^{12} cm^{-2} for CO_2, D_2O (substituted for H_2O for enhanced scattering contrast), and surfactant **1**, respectively. The SLD of D_2O is much higher than those of the other components, and as the surfactant **1** chains are expected to be swollen with CO_2, making its SLD even closer to that of the medium ($\Delta_2 \sim \Delta_s$), the main SLD difference (or contrast) is between the core and the solvent. Thus, the SANS data mainly reflect the core (D_2O) dimensions, and for relatively monodisperse particles in the dilute solution limit, where particle−particle interactions may be neglected to a first approximation, $P(Q)$ may be approximated[21] by $P(Q) \sim \exp[(-QR_g)^2/3]$. R_g is the radius of gyration, that is, the root-mean-square (rms) distance of all scattering elements from the center of gravity, where the summation runs over all scattering elements, k. Thus, a (Guinier) plot of $\ln[I(Q)]$ versus Q^2 should be linear, with slope $(R_g^2)/3$.

Figure 2 depicts an example of a SANS profile for water in supercritical CO_2 microemulsion stabilized by surfactant **1** (2.7 wt %) at a water loading with a corrected ratio of $W_0 = 10$ at 414 bar and 35 °C. In the inset, the data are shown in corresponding Guinier plots, from which an R_g value of 23.0 Å [$I(0) = 0.35 \pm 0.03$ cm^{-1}] was determined. The R_g is relatively independent of concentration and changes by ~12% as the surfactant concentration is increased from 2.7 to 5.3 wt %, with the same ratio of surfactant/D_2O and a corresponding increase in the volume fraction of D_2O from 0.75% to 1.5%. This indicates that the use of the Guinier approximation is reasonable to a first approximation. It has previously been shown that the majority of the scattering arises from D_2O,[4] and the corresponding core radius [$R = (5/3)^{0.5}R_g$] is 29.7 Å for the particles represented in Figure 2.

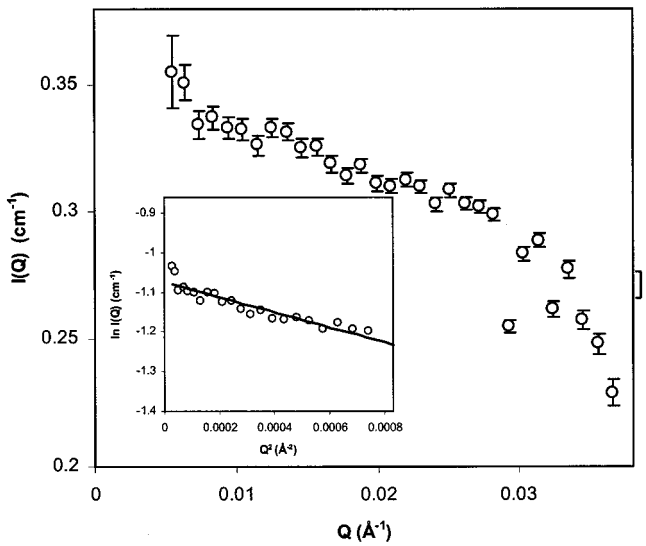

Figure 2. SANS profile of surfactant **1** in supercritical CO_2 (2.7 wt % surfactant **1**, corrected $W_0 = 10$, at 414 bar and 35 °C). The corresponding Guinier plot is shown in the inset.

Molecular Dynamics Simulation

We used the united atom force field to model the chains of the surfactant molecule (under this description, every CH_2, CF_2, and CF_3 group was represented as one pseudo-atom). Every atom in the headgroup was described explicitly. A set of partial atomic charges was determined via quantum electronic structure calculations on the surfactant molecule. Using the Gaussian 98 program[22] with the 6-31+G* basis set, we performed a Hartree−Fock geometry optimization procedure. The atom-centered point charges were determined via fits to the electrostatic potentials obtained from the calculated wave functions. These are shown in Figure 1. The fluorinated tails of surfactant molecules were described by a potential model proposed by Cui et al.[23] The potential parameters from this model can be found in Table 1 of ref 14. To describe the dihedral (δ =CF_2−CH_2−CH_2−O), we followed the procedure from ref 24. We started with a model compound (CF_2H−CH_2−CH_2−O)(CH_3−O)PO_2^- and used the Gaussian 98 program to compute the ab initio energy profile for this compound as a function of the dihedral angle δ. For each optimized geometry corresponding to a particular value of δ, an energy minimization neglecting the contribution from our dihedral of interest was performed using the SANDER module of AMBER 6.0.[25] Finally, the difference in energy between the ab initio and SANDER calculations was fitted to the function

$$V_{dih} = \frac{1}{2}\sum_n V_n(1 + \cos(n\phi - \gamma)) \quad (2)$$

to get the dihedral angle parameters which are tabulated in Table 1. The OPLS parameters[26] were used for the rest

(16) *Neutronenstreuexperimente am FRJ2 in Jülich*; Forschungszentrum Jülich GmbH: Jülich, Germany, 1997; English and German texts are available.

(17) McClain, J.; Londono, J. D.; Chillura-Martino, D.; Triolo, R.; Betts, D. E.; Canelas, D. A.; Cochran, H. D.; Samulski, E. T.; DeSimone, J. M.; Wignall, G. D. *Science* **1996**, *274*, 2049.

(18) Triolo, F.; Triolo, A.; Triolo, R.; Londono, J. D.; Wignall, G. D.; McClain, J. B.; Betts, D. E.; Wells, S.; Samulski, E. T.; DeSimone, J. M. *Langmuir* **2000**, *16* (2), 416.

(19) Wignall, G. D.; Bates, F. S. *J. Appl. Crystallogr.* **1986**, *20*, 28.

(20) Wignall, G. D. In *Physical Properties of Polymers Handbook*; Mark, J. E., Ed.; AIP Press: Woodbury, New York, 1996; p 299. Guinier, A.; Fournet, G. *Small-Angle Scattering of X-rays*; Wiley: New York, 1955.

(21) Guinier, A.; Fournet, G. *Small-Angle Scattering of X-rays*; John Wiley: New York, 1955.

(22) Frisch, M. J.; Trucks, G. W.; Head-Gordon, M.; Gill, P. M. W.; Wong, M. W.; Foresman, J. B.; Johnson, B. G.; Schlegel, H. B.; Robb, M. A.; Replogle, E. S.; Gomperts, R.; Andres, J. L.; Raghavachari, K.; Binkley, J. S.; Gonzalez, C.; Martin, R. L.; Fox, D. J.; Defrees, D. J.; Baker, J.; Stewart, J. J. P.; Pople, J. A. *Gaussian 98*, revision A.6; Gaussian, Inc.: Pittsburgh, PA, 1998.

(23) Cui, S. T.; Siepmann, J. I.; Cochran, H. D.; Cummings, P. T. *Fluid Phase Equlib.* **1998**, *146*, 51−61.

(24) Smondyrev, A. M.; Berkowitz, M. L. *J. Comput. Chem.* **1999**, *20*, 531−545.

(25) Case, D. A.; Pearlman, D. A.; Caldwell, J. W.; Cheatham, T. E., III; Ross, W. S.; Simmerling, C. L.; Darden, T. A.; Merz, K. M.; Stanton, R. V.; Cheng, A. L.; Vincent, J. J.; Crowley, M.; Tsui, V.; Radmer, R. J.; Duan, Y.; Pitera, J.; Massova, I.; Seibel, G. L.; Singh, U. C.; Weiner, P. K.; Kollman, P. A. *AMBER 6*; University of California: San Francisco, 1999.

(26) Jorgensen, W.; Tirado-Rives, J. *J. Am. Chem. Soc.* **1988**, *110*, 1657−1666.

Table 1. Potential Parameters for the Dihedral Angle

dihedral	$V_n/2$ (kcal/mol)	γ (deg)	n
OS−CH_2−CH_2−CF_2	2.732	0.0	3
	−1.099	30.0	1

of the intermolecular and intramolecular interactions present in the surfactant. The SPC/E water model[27] and a single-site CO_2 model[28] were among the other models used in the simulation. Since fluorinated tails of surfactant molecules were represented by uncharged united atoms, we decided that an uncharged united atom representing a CO_2 molecule will be a consistent choice. The single-site CO_2 model was tested to make sure that it reproduces the equation of state in the supercritical region. As we can see from Figure 3, where we show the pressure dependence of supercritical CO_2 on density for (a) experiment, (b) a more sophisticated EPM2 model[29] (a three-site model, with a partial charge on every site), and the single-site Lennard-Jones model that we used, the simple model does as good a job as a more sophisticated EPM2 model in the description of the pressure density dependence in the supercritical region.

The system we simulated contained 1616 water molecules, 160 surfactant molecules, and 6991 CO_2 molecules in a cubic box at $T = 35°$ C and at pressure $P = 414$ bar. These values for the temperature and pressure are the same as the values present in the SANS experimental study described in the previous section. We started our simulation from a starting configuration represented by an aggregate in which we distributed the surfactant molecules around the periphery of a sphere of radius 23 Å pointing the monomer heads inward and the tails outward. Extensive equilibration and thermalization of this highly ordered structure were performed, keeping the phosphorus atoms fixed to remove the initial strain. After that, we added water molecules and Na^+ ions to the empty space inside the sphere and performed another set of minimization and thermalization runs, this time letting the phosphorus atoms go free. The obtained structure was then inserted into the hole made in the middle of a cubic box containing CO_2 molecules at the density of 1 g/mL. The final set of minimization and thermalization runs was performed before a 200 ps equilibration run in the NPT ensemble. This last simulation provided the initial conditions for the production run of 4 ns in the NPT ensemble. Both the thermostat and barostat relaxation times were set to 0.5 ps, and a 2 fs time step was used. Periodic boundary conditions were applied in all three dimensions, and a smooth particle mesh Ewald (SPME)[30] method was used for calculations of electrostatic contributions. The simulations were carried out using the DLPOLY molecular dynamics simulation package.[31]

One of the primary characteristics of a reverse micelle is its size. The radius of gyration of the aqueous core is very often used as a quantity that describes this characteristic. Therefore, we calculated this quantity by using the following expression

$$R_g^2 = \sum_i m_i(r_i - r_0)^2 / \sum_i m_i \qquad (3)$$

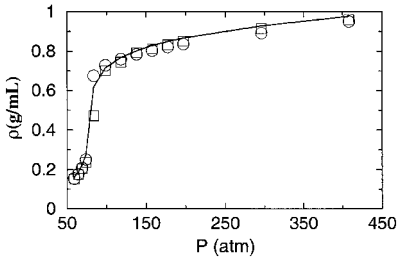

Figure 3. Pressure dependence of supercritical CO_2 on density for experiment (solid line), EPM2 model (squares), and single-site Lennard-Jones model (circles).

where the index i includes water molecules, Na^+ ions, headgroups, and two CH_2 groups in each tail since they were found to be in contact with water. m_i is the mass, and r_i is the distance of atom i from the center of mass r_0. The value of R_g we obtained from the simulation was 24.3± 2 Å, which is in reasonable agreement with the experimental finding.

To determine the surface area per headgroup available for interaction with water, we used the method of Lee and Richards.[32] In this method, all of the sodium and water molecules were removed from the system and a probe molecule was rolled across the surface of the micelle and the contact area was summed to quantify the total accessible surface area. A 1.4 Å probe was utilized to mimic the water in the system. We obtained an available area per headgroup of $A_h = 64.5 \pm 2$ Å^2. It is useful and instructive to compare the area per headgroup we obtained for surfactant **1** and the area per headgroup for some other surfactants in W/C microemulsions. Thus Eastoe et al.[9] found that for fluorinated sulfosuccinate surfactants the area per headgroup is ∼115 Å^2 in a W/C microemulsion. This value is much larger than the value we report here for surfactant **1**. One is tempted to explain the observed difference in the areas as due to the difference in the size of the headgroup: the sulfosuccinate surfactant has a larger headgroup compared to a phosphate-based surfactant. Nevertheless, this explanation is not satisfactory since the area of the headgroup is unchanged (∼64 Å^2) when going from sulfosuccinate to phosphate-based surfactants in the case of water/oil (W/O) microemulsions.[33,34] A deeper understanding of the differences in the properties of W/O and W/C microemulsions is needed to explain the variation in the areas per headgroup.

One can estimate the area per headgroup of a phosphate-based surfactant by using the equation connecting the radius of the water core R_c, the volume of the water molecule V_w, and the volume of the headgroup V_h:[34]

$$R_c = \frac{3V_w}{A_h}W_0 + \frac{3V_h}{A_h} \qquad (4)$$

For surfactant **1**, we use the value of 29.7 Å for R_c that we obtained from SANS experiments and assume that the headgroup is a sphere of radius 4.0 Å. With this input, eq 4 predicts that the area per headgroup for our surfactant is 57.1 Å^2. We can also estimate the area per headgroup of a phosphate-based surfactant used in the recent experiment of Steytler et al.[12] Since that surfactant has

(27) Berendsen, H. J. C.; Grigera, J. R.; Straatsma, T. P. *J. Phys. Chem.* **1987**, *91*, 6269−6271.
(28) Higashi, H.; Iwai, Y.; Uchida, H.; Arai, Y. *J. Supercrit. Fluids* **1998**, *13*, 93−97.
(29) Harris, J. G.; Yung, K. H. *J. Phys. Chem.* **1995**, *99*, 12021−12024.
(30) Essmann, U.; Perera, L.; Berkowitz, M. L.; Darden, T.; Lee, H.; Pedersen, L. G. *J. Chem. Phys*. **1995**, *103*, 8577−8593.
(31) Smith, W.; Forester, T. R. *DLPOLY*, version 2.12; CCLRC, Daresbury Laboratory: Daresbury, Cheshire, U.K., 1999.
(32) Lee, B.; Richards, F. M. *J. Mol. Biol.* **1971**, *55*, 379.
(33) Steytler, D. C.; Sargeant, D. L.; Welsh, G. E.; Robinson, B. H.; Heenan, R. K. *Langmuir* **1996**, *12*, 5312−5318.
(34) Nave, S.; Eastoe, J.; Heenan, J. K.; Steytler, D.; Grillo, I. *Langmuir* **2000**, *16*, 8741−8748.

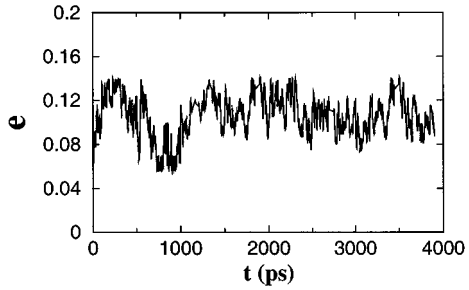

Figure 4. Eccentricity of the aggregate as a function of time.

one less methyl group, we can assume that the headgroup is smaller in this case and use a value of 2.5 Å for its radius. The value of R_c was provided in ref 12, and it is 17 Å. Using these data, we get from eq 4 that the area per headgroup for the phosphate-based surfactant in Steytler et al.'s experiment is 64.5 Å^2. As we can see, the estimates for the area per headgroup of phosphate-based surfactants are in qualitative agreement with the value we obtained in our simulation. This agreement should not be overemphasized, since we used eq 4 for just one value of W_0 and we do not know how good the linearity of the plot of R_c versus W_0 is. Moreover, it seems that due to the contrast in the system in the experimental work of Steytler et al., we do not need to include the last term from eq 4. Without this term, we get an area per headgroup of only ~53 Å^2.

To characterize quantitatively the shape of the aggregate, we calculated the eccentricity of the micelle core. The eccentricity is defined as[14]

$$e = 1 - \frac{I_{\min}}{I_{\text{avg}}} \tag{5}$$

where $I_{\min}$ is the moment of inertia along the x, y, or z axis with the smallest magnitude and I_{avg} is the average of all three moments of inertia. We used the same atoms to calculate the moments of inertia as the one we used to calculate the radius of gyration. For a perfect sphere, the eccentricity should be zero. The value of e for our micelle was 0.095 ± 0.04. This value shows that the micelle in our simulation is not a perfectly spherical object. We also observed that the aggregated core is stable, since the value of the eccentricity was rather stable in time, especially during the time period of 1−4 ns (see Figure 4). Thermal fluctuations of the micelle are dictated not just by the temperature but also by interfacial tensions in the system. These depend on the model potentials, and it will be interesting to study how models of different sophistication influence the fluctuation character of the micelle.

A snapshot picture of a cross section of our system at 4 ns is shown in Figure 5. The figure shows that the headgroups are distributed at the surface of the aqueous core. The observed distribution of Na^+ ions indicates the possibility of ion pair formation between Na^+ and the headgroups. The tails of the surfactants are extending out and are solvated in CO_2.

Figure 6 shows the density of constituents in our system measured as a function of distance from the core center.

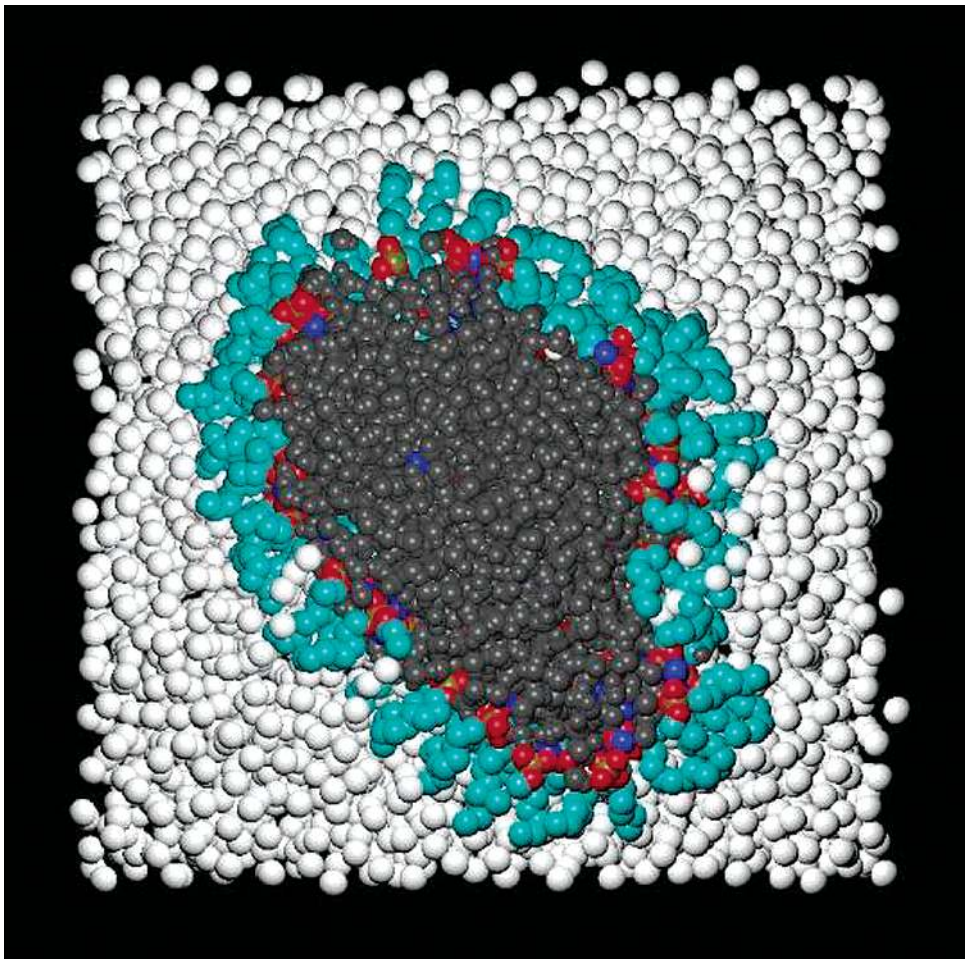

Figure 5. Snapshot of a cross section of the system at 4 ns. The color scheme is white for CO_2, green for surfactant tails, red for phosphate oxygen, gold for phosphorus, blue for Na^+, and gray for water.

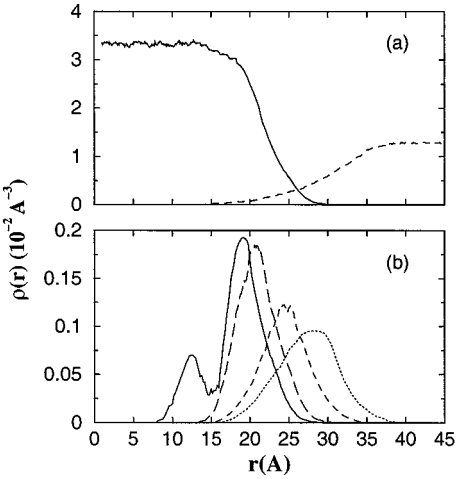

Figure 6. The number density profile of (a) water (solid line) and carbon dioxide (dashed line) and (b) sodium (solid line), headgroup phosphorus (long-dashed line), tail CH_2 (short-dashed line), and tail CF_2 (dotted line) as a function of distance from the center of the aqueous core.

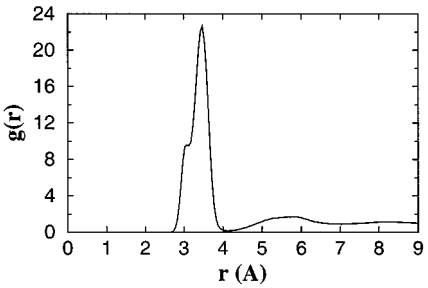

Figure 7. The pair radial distribution function for Na^+-P.

This figure shows the existence of an aqueous core region, regions of interface between the water core and the headgroups, and another region of interface between the tails and carbon dioxide. As we can see, the interfacial regions are rather wide, and this is consistent with the observations made in other simulations on micellar systems.[14] To learn more details about the structural properties of our reverse micelle, we consider various pair radial distribution functions (rdf) and associate coordination numbers. In Figure 7, we plotted the rdf for the Na^+-phosphorus (P) pair. As we can see, the first peak in the rdf has its maximum at a distance of 3.35 Å and a small shoulder at a shorter distance. The appearance of this shoulder is probably due to the formation of a stable site for Na^+ by the pair of oxygens attached to phosphorus. An average of 90% of sodium ions are found to be within the first shell of the headgroup, thus confirming the presence of contact-ion pairs in our system. The remaining 10% of the ions are located in the region where the second peak in the rdf is seen, thus forming solvent-separated ion pairs, or further away, by dissociating from the surface altogether. During the simulation run, we observed that the average percentage of sodium ions in the first shell varied between 88 and 91%. The calculated coordination number was 1.10, which means that there is some bridging between the Na^+ ions and phosphorus.

The rdf's for $Na-O_w$ (water oxygen) and $P-O_w$ are shown in Figure 8. The Na^+-O_w pair distribution function shows a distinct first hydration shell with a peak maximum at 2.37 Å and a weak second peak at 4.62 Å. The sharp first peak in the Na^+-O_w rdf and the near-zero density in the region between the first and second solvation shells reflect the much stronger interaction that exists between water

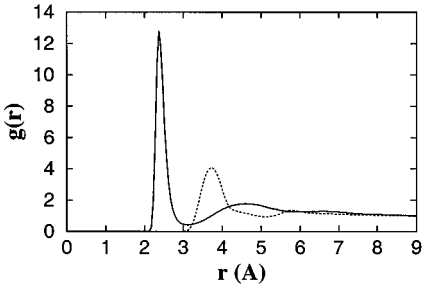

Figure 8. The pair radial distribution function for Na^+-O_w (solid line) and $P-O_w$ (dotted line).

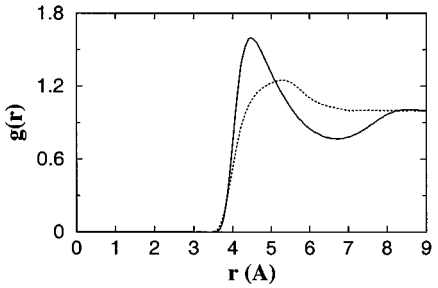

Figure 9. The pair radial distribution functions for CF_3-CO_2 (solid line) and CF_2-CO_2 (dashed line). CF_3, CF_2, and CO_2 are given in united atom representation. The CF_2 group is the one closest to the headgroup of the surfactant molecule.

and the relatively small cations. The coordination number of the first solvation shell is calculated to be 3.5 compared to the value of 5.8 at infinite dilution,[35] which confirms the presence of contact-ion pairs between the phosphate groups and Na^+ counterions in our system. The rdf for $P-O_w$ in contrast shows a small but broad first peak and a smaller second peak. The number of water molecules in the first hydration shell is 7.9, which implies that there is substantial overlap of the P hydration shells. A more detailed description of the water structure and dynamics in the hydration pool of our reverse micelle will be given elsewhere.[36] In Figure 9, we display the radial distribution function between the terminal group CF_3 in the surfactant chain and CO_2 and the radial distribution function between the CF_2 group closest to the headgroup in the chain and CO_2. As we can clearly see from the figure, both CF_3 and CF_2 groups are solvated, although the terminal CF_3 group is solvated more strongly by carbon dioxide.

Conclusions

The existence of microemulsions in the system composed of phosphate-based surfactant **1**, water, and supercritical CO_2 was demonstrated by SANS experiments. Molecular dynamics simulations performed under the same conditions as in the SANS experiments show that the reverse micelle constructed in the simulation is stable over a time period of 4 ns. We observed that the values of the radius of gyration extracted from the experiment and from simulation are in reasonable agreement, given the level of assumptions and approximations used in the interpretations of the data. Molecular dynamics simulation provides us with a number of details about the micelle geometry and structure. We calculated that the area per headgroup for our surfactant is ~64 Å^2. This value is in good agreement with the value that can be extracted by analyzing recent SANS experiments performed on a

(35) Koneshan, S.; Rasaiah, J. C.; Lynden-Bell, R. M.; Lee, S. H. *J. Phys. Chem. B* **1998**, *102*, 4193−4204.
(36) Senapati, S.; Berkowitz, M. L. Manuscript in preparation.

similar surfactant. The calculation of micelle eccentricity indicates that the micelle has a slightly nonspherical shape. Direct observation of micelle shape fluctuations and the time behavior of eccentricity indicate stability of the micelle shape on the time scale of the simulation. To get a feeling for the possible changes in micelle shape, we performed simulated annealing on the micelle. The shape and the energy of the micelle after annealing were similar to those prior to annealing. We also observed from the molecular dynamics that counterions are strongly bound to headgroups and that water solvates the headgroups and carbon dioxide solvates the tails. The study of the structure and dynamics of water in the aqueous core will be the subject of a future publication.

Acknowledgment. This work was supported by the Kenan Center for the Utilization of Carbon Dioxide in Manufacturing and the STC Program of the National Science Foundation under Agreement CHE-9876674. The research at Oak Ridge was supported by the Division of Materials Sciences, under Contract No. DE-AC05-00OR22725 with the Oak Ridge National Laboratory, managed by UT-Battelle, LLC. We wish to thank Professor D. Richter for the hospitality and assistance provided by the staff of FZJ and the Alexander von Humboldt-Stiftung for support to Y.B.M. The simulations were performed on an IBM SP at the North Carolina Supercomputing Center.

LA025952S